TÜBİTAK

Turkish Journal of Earth Sciences

http://journals.tubitak.gov.tr/earth/

Research Article

Turkish J Earth Sci
(2019) 28: 920-938

doi:10.3906/yer-1809-34

Mineralogy, petrology and geochemistry of mafic dikes in the southeast Jebal-E-Barez Granitoids (Bam, Kerman province, Iran): Studies from mafic dikes formed in a volcanic arc-setting

Shirin BEHPOUR[1,*], Abbas MORADIAN[1], Hamid AHMADIPOUR[1], Kazuo NAKASHIMA[2]
[1]Department of Geology, College of Sciences, Shahid Bahonar University, Kerman, Iran
[2]Department of Earth and Environmental Sciences, Yamagata University, Yamagata, Japan

Received: 28.09.2018 • **Accepted/Published Online:** 25.04.2019 • **Final Version:** 07.11.2019

Abstract: In the southeastern part of the Jebal-E-Barez Oligocene granitoids (Kerman province, Iran), there are numerous mafic dikes and this work attempts to investigate the petrological, geochemical and mineral chemistry of these dikes. The dikes clearly follow faults which trend mainly N50-70W and N20-40W. Their thicknesses vary from 1 cm to 3 m and their contacts with the host granitic rocks are sharp without any extensive contact metamorphism which may be due to the lack of magmatic fluids. The Jebal-E-Barez mafic dikes contain plagioclase, clinopyroxene and amphibole as major minerals and overall show porphyritic texture, but intergranular, ophitic and subophitic textures are also visible. The amphiboles are classified mainly as paragasite and tschermakite. These are magmatic, as indicated by Si content of the studied mafic dikes. Based on Al-in-hornblende geothermobarometry, average crystallization pressures are estimated from 5.25 to 7.07 kbar and temperatures from 867 to 872 °C. Thermobarometric estimations show temperatures of 1000 ± 200 °C and depth of 30–40 km for crystallization of the clinopyroxenes. Chemical composition of the amphiboles suggests the parent magmas of the mafic dikes derived from a mantle source. Whole rock geochemistry data reveal that the studied dikes belong to the calc-alkaline magma series. They are enriched in light rare earth elements (LREE) and large ion lithophile elements (LILE) such as Cs, Rb, Ba, and Sr, with negative anomalies for high-field-strength elements (HFSE) such as Nb and Ta. The weak negative Eu anomaly is evidence of a slightly earlier separation of a mineral phase such as plagioclase. According to trace element abundances, Ba/Nb, Ce/Yb, and Zr/Y ratios, and tectono-magmatic discrimination diagrams, the primitive magma derived from an enriched garnet-free mantle source, contaminated by the crust and emplaced in continental arc environment.

Key words: Mafic dikes, mineral chemistry, petrology, calc-alkaline, geothermobarometer, continental arc, Central Iran

1. Introduction

Petrogenesis and geodynamic characteristics of mantle-sourced mafic dikes provide important information about tectono-magmatic evolution of orogenic belts (Gorring and Kay, 2001; Yang et al., 2007; Wang et al., 2009). Mafic dikes can be sourced from asthenospheric mantle related to mantle plumes, subduction and rift activities (Hoek and Seitz, 1995; Buchan et al., 2006; Xu et al., 2017). These shallow masses intrude into the continental lithosphere through extensional fractures in various extensional settings such as midocean spreading ridges (Robinson et al., 2008), back-arc, and post-collisional tectonic regimes (Taylor and Martinez, 2003; Xu et al., 2012).

Numerous studies have been performed on mafic dikes in Iran (Arvin and Robinson, 1994; Allahyari et al., 2010; Saccani et al., 2013). According to these studies, diabase dikes (Berberian and King, 1981; Bagheri and Stampfli, 2008; Moghadam et al., 2013) and lamprophyre dikes (Torabi, 2010; Bayat and Torabi, 2011; Torabi, 2011; Pandey et al., 2017) are the most abundant types of dikes in Central Iran.

The diabase mafic dikes in this study are located in Central Iran in the southeast of the Urumieh-Dokhtar Magmatic Assemblage (UDMA), which extends to Kerman province where it is referred to as the Dehaj-Sarduieh volcano-plutonic belt. These dikes were injected into the Jebal-E-Barez granitoid (JBG) after extensive Eocene magmatism.

Due to a lack of studies about these dikes, the present work aims to determine petrographical and petrological characteristics along with mineral chemistry of these diabase dikes in JBG. For this purpose, the study was organized into four phases: 1) investigating parental magma composition, 2) specifying petrogenesis processes,

* Correspondence: sh.behpour@sci.uk.ac.ir

3) defining tectonic settings and evolution of lithospheric mantle, and 4) estimating the depth of the magma chamber. Furthermore, we aim to provide new insights into Eocene magmatic processes in the region.

2. Geological setting

Convergence of the Iranian and Arabic plates in the late Mesozoic and continuation in the Early Cenozoic led to subduction of oceanic crust below Central Iran (Stöcklin, 1974; Agard et al., 2011; Castro et al., 2013, Sarjoughian and Kananian, 2017). The convergence caused extensive magmatism along the Sanandaj-Sirjan and Urumieh-Dokhtar belts in the Mesozoic and Tertiary, respectively (Agard et al., 2011).

The studied dikes and the host granitic rocks are located along the UDMA in Central Iran (Stocklin and Nabavi, 1973). Magmatic activity in this zone began with volcanic eruptions in Late Jurassic which peaked in the Eocene (Berberian and King, 1981; Berberian et al., 1982). The studied dikes crop out in the JBG and are located southwest of Bam city (E 58°00′ to 58° 45′ and N 28°15′ to 29°00′) (Figure 1) (Sohrabi et al., 2015; Dimitrijevic, 1973). The JBG, with an area of 14 km (NW–SE) × 45 km (N–S), belongs to the Oligocene period (Stocklin and Nabavi, 1973), so these dikes are younger than Oligocene (Figure 2a). The JBG generally intrudes into Eocene volcanic rocks and the main lithologies are granodiorite and granite. The formation of the JBG complex was followed by the extension of volcanic complexes during the Eocene (Razak complex) and Oligocene (Hezar complex), which contain andesite, trachyandesite, trachybasalt, andesite–basalt, and acidic tuff (Shafiei et al, 2009).

These mafic dikes follow N50–70W and N20–40W trends (Figure 1c) and are 50 cm to 3 m in width and 10 m or longer in length. Based on field observations, the dikes exhibit porphyry to fine-grained textures and dark gray to dark green colors. The dikes are only slightly altered and in some cases, pyrites are visible to the naked eye. There are very dark green duplicate dikes in this complex which injected into other dikes (Figure 2b), and have finer grains than those of the host dikes.

The boundary between the dikes and their host rocks has no reaction rims, indicating a lack of magmatic fluids (Figures 2c and 3a). Numerous joints and faults across the studied area imply high tectonic activity in the region. The faults and fractures developed along the same trends as the dikes.

3. Analysis methods

Within the scope of this study, 80 thin sections were prepared for microscopic studies. Ten fresh samples selected for whole-rock geochemical analyses were crushed and powdered in an agate mill. Then, 0.2 g of the sample was added to 0.9 g lithium metaborate flux and mixed well before being fused in a furnace at 1000 °C. The resulting melt was then cooled and dissolved in 100 mL of 4% HNO_3 and 2% HCl solution and major and trace elements were analyzed by inductively coupled plasma-mass spectrometry (ICP-MS) and inductively coupled plasma atomic emission spectroscopy (ICP-AES) at the ALS Chemex laboratory in Canada. The analysis results are presented in Table 1.

Electron microprobe analysis of minerals was performed using an automated JEOL JXA-8900 microprobe (Yamagata University) at an accelerating voltage of 15 kV, a beam current of 20 nA, a beam diameter of about 5 μm, detection limit of 0.05 wt.%, and a maximum counting interval of 40 s. The diameter of the focused electron beam was about 5 μm. Data were processed by an online computer equipped with XM-86 PAC Software (JEOL) with the oxide ZAF method implemented. Calibration standards for the mentioned minerals were apatite, wollastonite, albite, adularia, synthetic SiO_2, TiO_2, Al_2O_3, Fe_2O_3, MnO, MgO, CaF_2, and NaCl. For each sample, several grains and several points on each mineral were analyzed based on textural relationships, and average values of the analytical results were taken as representative of typical composition of that mineral in each sample. The results of analyses for each mineral are shown in individual tables. Formula calculations for feldspar, amphibole and pyroxene are based on 8, 23, and 6 atoms of oxygen, respectively.

4. Results

4.1. Petrography

Host granitic rock units are composed of granodiorite and granite. Plagioclase (35%), quartz (25%), K-feldspar (20%), amphibole (10%), and biotite (7%) are the main minerals in granodiorite. Apatite, zircon and opaque minerals are accessory minerals. Granitic rocks, on the other hand, are mainly composed of K-feldspar (30%), plagioclase (25%), quartz (25%), biotite (10%), and amphibole (8%), with apatite, zircon, titanite, and opaque minerals as accessory mineral constituents. The granitoids exhibit a subhedral granular texture.

According to the results of petrographic studies, diabase dikes exhibited no obvious evidence of deformation and metamorphism. The samples show an aphanitic matrix and diabase textures and they exhibit ophitic and subophitic texture (Figure 3b) (Kretz, 1983). In terms of composition, the diabase dikes are made up of plagioclase (50%), clinopyroxene (25%), K-feldspar (10%), and anhedral quartz (less than 5%). Some samples contained amphibole (10%) (Figure 3c). The plagioclase is found both as phenocrysts and microlites. The phenocrysts of

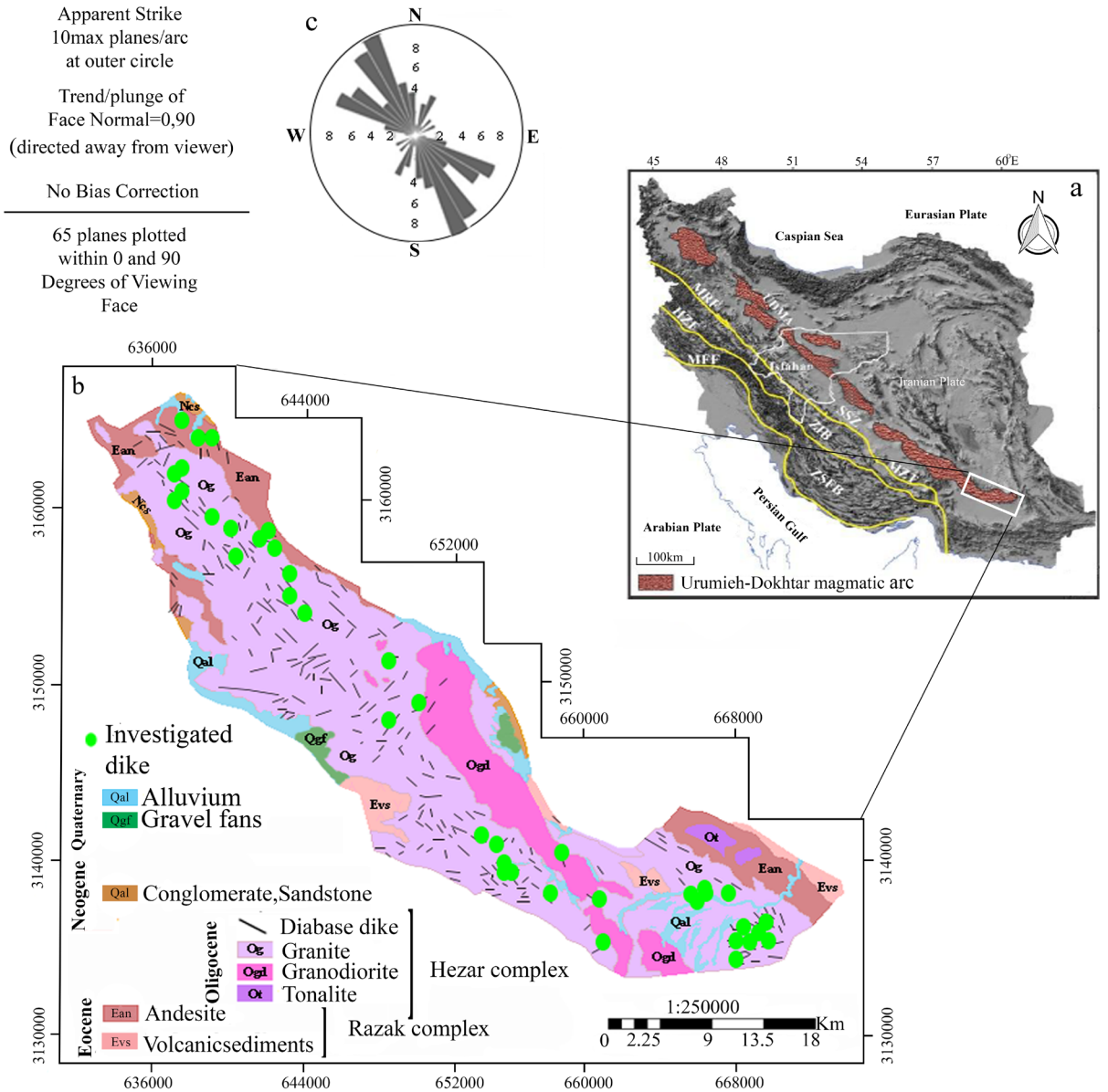

Figure 1. Map of the studied area, showing (a) Main tectonic units of Iran. Tectonic zones of the Zagros Orogen: ZSFB - Zagros Simply Folded Belt, ZIB - Zagros Imbricate Belt (High Zagros Belt), SSZ Sanandaj-Sirjan Zone, UDMA - Urumieh-Dokhtar Magmatic Arc, MFF Mountain Frontal Fault, MRF Main Recent Fault, HZF High Zagros Fault. Major faults: MZT - Main Zagros Thrust (Sohrabi et al., 2015 and references therein), (b) Simplified geological map of the studied area (Dimitrijevic, 1973), and (c) Rose diagrams of the dikes.

plagioclase are 1–4 mm in size (Figure 3d). The subhedral clinopyroxene phenocrysts range between 2 and 4 mm in size. These phenocrysts are augitic in composition and are located in a fine-grained matrix made of plagioclase laths, small clinopyroxene grains, and opaque minerals. Accessory minerals are apatite, zircon and opaque minerals. The suite of secondary minerals includes epidote, sericite, calcite, zeolite and chlorite. Microscopic studies show that the dominant texture of rocks in this area is porphyry, and intergranular in some cases.

4.2. Mineral chemistry

The major element composition of clinopyroxenes, plagioclase, and amphibole are presented in Tables 2, 3, and 4, respectively.

Clinopyroxenes exhibit augitic composition ($Wo_{27.71-28.85}$, $En_{42.70-48.13}$, $Fs_{23.28-29}$) (Figure 4a). They plot in the Ca-Na

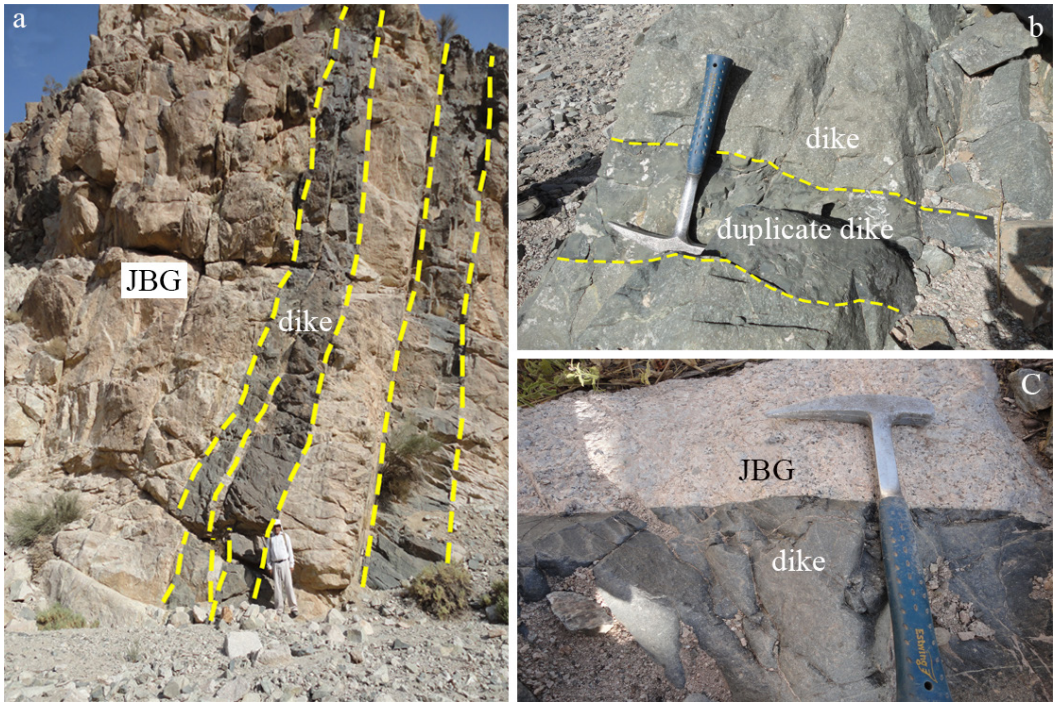

Figure 2. a) The studied dikes outcropping in the Jebal-E-Barez granitoid (JBG). b) Duplicate dikes injecting into other dikes, are finer grained than those of host dikes. c) The boundary between the dikes and their host rocks has no reaction margin.

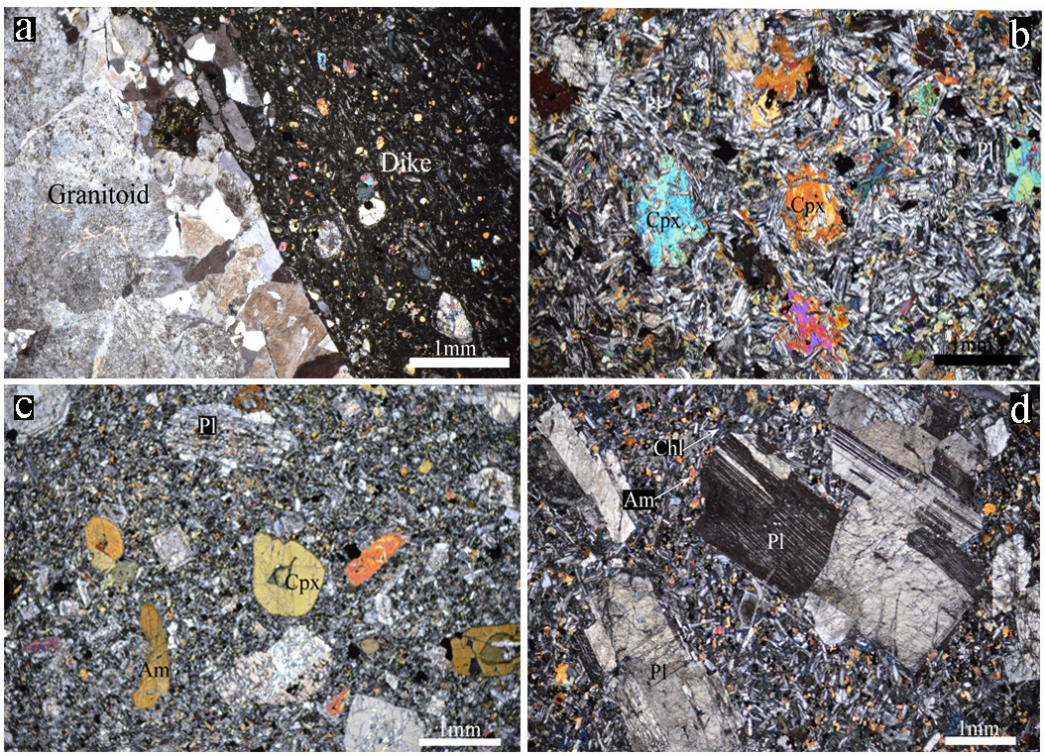

Figure 3. Representative photomicrographs of petrographic features of the JBG mafic dikes, cross-polarized light: a) the contact between the dikes and host rock, b) ophitic and sub-ophitic texture in dikes, c) primary amphibole in dikes, d) phenocrysts and microlites of plagioclase in dike. Clinopyroxene (Cpx), amphibole (Am), plagioclase (Pl), chlorite (Chl) (Kretz, 1983).

Table 1. Chemical composition of the JBG mafic dykes.

Samples	1jb8	2jb20	2jb33	2jb35	3jb14	3jb9	5jb16	5jb29	6jb15	9jb3
SiO_2 (wt.%)	46.80	48.00	48.50	46.30	48.90	50.00	49.00	47.80	48.00	50.20
TiO_2	0.90	0.99	0.96	1.01	0.89	0.76	0.78	0.82	0.81	0.70
Al_2O_3	17.40	18.45	18.45	16.65	17.60	18.95	18.65	17.35	19.25	17.25
$Fe_2O_3^T$	10.65	11.65	11.75	10.50	11.10	9.61	11.25	9.67	10.05	9.92
MnO	0.23	0.18	0.23	0.20	0.20	0.19	0.19	0.17	0.18	0.23
MgO	6.19	4.82	4.68	8.34	5.46	3.78	4.25	6.79	5.40	6.36
CaO	9.72	8.27	8.43	10.65	9.30	9.55	8.02	8.85	10.10	9.42
Na_2O	2.48	2.99	2.38	1.76	2.39	2.40	2.83	2.65	2.30	2.26
K_2O	0.95	0.97	0.86	0.95	0.60	0.80	0.80	1.04	0.72	0.65
P_2O_5	0.28	0.16	0.13	0.34	0.17	0.13	0.15	0.17	0.14	0.12
Cr_2O_3	0.02	<0.01	<0.01	0.05	<0.01	<0.01	<0.01	0.02	0.01	0.01
Total	98.27	98.87	98.82	99.92	99.84	100.55	98.46	98.40	99.19	99.31
Mg#	36.76	29.27	28.48	44.27	32.97	28.23	27.42	41.25	34.95	39.07
Ba (ppm)	199	233	251	170.5	149	261	171.5	227	161.5	191.5
Ce	30.7	16.1	16.5	42.4	25.1	22.1	19.5	26.8	19.9	17.1
Cr	120	20	10	360	20	10	<10	180	60	50
Cs	0.84	0.85	1.04	1.2	2.29	2.15	2.11	1.05	0.7	0.92
Cu	74	118	96	55	86	93	118	77	78	41
Dy	3.49	3.31	3.33	3.78	3.98	3.38	3.53	3.29	3.03	2.82
Er	2.1	2.04	2.04	1.99	2.46	2.05	2.19	1.98	1.83	1.75
Eu	1.11	0.96	0.88	1.36	1.04	0.89	1.01	0.97	0.87	0.74
Ga	19.2	19.7	14.8	16	17.4	16.6	16.6	16	16.9	15.3
Gd	3.68	3.47	3.16	4.42	4.12	3.47	3.6	3.32	3.28	2.73
Hf	2.5	1.8	1.8	3	2.9	2.6	2.1	2.1	1.9	2
Ho	0.75	0.7	0.7	0.77	0.85	0.71	0.77	0.72	0.63	0.62
La	13.9	6.8	7.2	20.2	11	10.3	8.5	12.5	9	7.7
Lu	0.28	0.28	0.3	0.27	0.35	0.33	0.39	0.29	0.27	0.26
Nb	6.2	2.5	2.9	10.8	4.5	3.7	3.2	4.1	2.9	3.2
Nd	16.4	11	10.1	20.8	14.1	12.2	11.5	13.6	11.4	8.9
Ni	45	<5	<5	123	16	5	<5	73	34	28
Pr	3.98	2.3	2.21	5.2	3.29	2.78	2.65	3.25	2.59	2.3
Rb	34.7	29.5	33	29.8	25.3	31.8	32.2	28	16.4	20.6
Sm	3.86	3.03	2.7	4.45	3.67	3.21	3.27	3.27	2.91	2.48
Sr	555	543	477	710	441	437	488	665	474	416
Ta	0.3	0.1	0.2	0.6	0.2	0.2	0.2	0.2	0.1	0.2
Tb	0.58	0.6	0.54	0.67	0.68	0.57	0.6	0.54	0.47	0.45
Th	1.19	1.07	0.97	2.06	1.95	2.19	1.36	2.42	1.59	1.93
Tm	0.31	0.28	0.31	0.3	0.38	0.34	0.36	0.28	0.3	0.26
U	0.37	0.32	0.43	0.74	0.56	0.69	0.47	0.6	0.43	0.52
V	220	298	278	203	271	239	257	272	292	253
Y	19.2	18.6	18.5	19.7	22.4	19.2	20.4	18.1	16.7	17.1
Yb	2.25	2.1	1.99	1.93	2.38	1.88	2.1	1.78	1.68	1.77
Zr	108	62	61	113	104	90	74	77	63	80
Eu/Eu^*	0.39	0.37	0.42	0.49	0.39	0.37	0.41	0.40	0.37	0.36
$(La/Sm)_n$	2.32	1.45	1.72	2.93	1.93	2.07	1.68	2.47	2.00	2.00
$(La/Yb)_n$	4.43	2.32	2.60	7.51	3.32	3.93	2.90	5.04	3.84	3.12

Table 2. Representative chemical composition and calculated mineral formulae of clinopyroxenes from the JBG mafic dikes. Formulae calculated on the basis of 6 oxygens.

Sample	b1	b2	b3	b4	b5	b6	d1	d2	d3	d4	d5	d6
Oxides (wt%)												
SiO_2	53.41	53.57	53.65	52.92	53.20	54.48	53.96	53.16	53.80	52.49	53.80	52.57
TiO_2	0.18	0.68	0.79	0.75	0.43	0.27	0.23	0.53	0.41	0.28	0.28	0.00
$A_{l2}O_3$	3.77	3.62	3.97	4.42	4.38	4.05	3.58	5.28	4.41	4.89	4.81	4.84
FeO	15.71	12.30	13.50	14.41	14.29	13.40	15.37	14.54	15.16	14.73	14.23	15.55
MnO	0.60	0.62	0.42	0.63	0.50	0.50	0.59	0.40	0.57	0.59	0.49	0.15
MgO	13.47	14.99	14.37	13.61	13.83	14.69	13.76	13.72	13.48	13.64	14.04	13.59
CaO	12.42	12.39	12.39	11.96	12.53	12.50	12.24	11.99	12.23	12.50	11.90	12.64
Na_2O	0.26	0.16	0.29	0.27	0.26	0.18	0.19	0.27	0.28	0.28	0.22	0.25
K_2O	0.15	0.09	0.09	0.12	0.17	0.15	0.08	0.13	0.13	0.14	0.08	0.17
Cr_2O_3	0.03	0.09	0.05	0.32	0.02	0.16	0.39	0.16	0.41	0.11	0.23	0.11
Total	99.99	98.51	99.52	99.40	99.62	100.37	100.39	100.16	100.88	99.64	100.07	99.86
Cations (apfu)												
Si	1.99	1.99	1.98	1.97	1.98	1.99	2.00	1.96	1.98	1.96	1.98	1.96
$Al_{(IV)}$	0.01	0.01	0.02	0.03	0.02	0.01	0.00	0.04	0.02	0.04	0.02	0.04
$Al_{(VI)}$	0.15	0.15	0.16	0.16	0.17	0.17	0.15	0.19	0.17	0.17	0.19	0.17
Al^T	0.17	0.16	0.17	0.19	0.19	0.17	0.16	0.23	0.19	0.21	0.21	0.21
Fe	0.49	0.38	0.42	0.45	0.44	0.41	0.48	0.45	0.47	0.46	0.44	0.48
Ti	0.01	0.02	0.02	0.02	0.01	0.01	0.01	0.01	0.01	0.01	0.01	0.00
Cr	0.00	0.00	0.00	0.01	0.00	0.00	0.01	0.00	0.01	0.00	0.01	0.00
Mg	0.75	0.83	0.79	0.76	0.77	0.80	0.76	0.75	0.74	0.76	0.77	0.75
Fe^2	0.40	0.38	0.39	0.40	0.39	0.39	0.40	0.41	0.40	0.40	0.41	0.41
Mn	0.02	0.02	0.01	0.02	0.02	0.02	0.02	0.01	0.02	0.02	0.02	0.00
Ca	0.50	0.49	0.49	0.48	0.50	0.49	0.48	0.47	0.48	0.50	0.47	0.50
Na	0.02	0.01	0.02	0.02	0.02	0.01	0.01	0.02	0.02	0.02	0.02	0.02
K	0.01	0.00	0.00	0.01	0.01	0.01	0.00	0.01	0.01	0.01	0.00	0.01
En	42.71	48.13	46.21	44.42	44.42	46.67	43.67	44.66	43.34	43.69	45.51	43.17
Fs	29.01	23.28	25.13	27.53	26.66	24.79	28.42	27.29	28.40	27.54	26.77	27.98
Wo	28.28	28.58	28.65	28.05	28.92	28.55	27.91	28.05	28.26	28.78	27.72	28.86

pyroxene area on the Q-J diagram (Figure 4b) (Morimoto, 1988). Chemical composition and the environment of dikes affected the clinopyroxene composition. According to Al_2O_3 vs. SiO_2, the magmatic series is subalkaline (Figure 4c) (Le Bas, 1962).

The phenocryst composition of the plagioclase changes from andesine to bytownite (An_{42-87}) (Figure 5a). Normal and oscillatory zoning is relatively common in the phenocrysts (Figure 5b). H_2O pressure (NBr and Son, 1992) and thermodynamic changes (Bottinga et al., 1966) in themagmatic system affects the composition and zoning of plagioclase during magmatic crystallization.

In the study area, amphiboles are found in both primary and secondary forms. Primary amphiboles are calcic and plot in the paragasite, sadanagaite, and tschermakite field (Hawthorne et al., 2012); on the other hand, secondary

Table 3. Representative chemical composition and calculated mineral formulae of plagioclases from the JBG mafic dikes. Formulae calculated on the basis of 8 oxygens.

Samples	2jb5-1	2jb5-2	2jb5-3	2jb4.1	2jb4.2	5jb-1	5jb-2	5jb3	5jb4	jb1	jb2	jb3	jb4	2jb6	2jb3	2jb35
Oxides (wt%)																
SiO_2	47.73	48.29	48.57	49.21	51.40	49.72	49.42	49.00	50.01	48.19	48.23	48.51	48.26	64.08	55.34	60.69
TiO_2	0.00	0.00	0.04	0.07	0.01	0.00	0.00	0.01	0.00	0.00	0.00	0.00	0.08	0.01	0.04	0.01
Al_2O_3	32.39	33.69	32.95	32.34	30.13	33.79	33.20	34.42	32.36	33.35	33.47	33.71	33.14	22.97	27.97	25.96
FeO	0.55	0.51	0.52	0.59	0.49	0.47	0.43	0.36	0.80	0.50	0.45	0.51	0.55	0.04	0.62	0.22
MnO	0.07	0.09	0.00	0.01	0.05	0.01	0.09	0.00	0.09	0.00	0.00	0.06	0.00	0.03	0.00	0.02
MgO	0.05	0.09	0.08	0.06	0.10	0.32	0.14	0.04	0.54	0.05	0.05	0.08	0.06	0.00	0.04	0.00
CaO	17.59	17.08	16.29	15.62	15.43	14.24	14.05	15.49	13.33	17.47	17.18	16.97	16.30	3.73	10.88	7.12
Na_2O	1.55	1.52	1.76	2.14	2.85	1.50	1.57	1.61	2.47	1.34	1.34	1.39	1.30	9.91	5.46	5.33
K_2O	0.11	0.11	0.13	0.15	0.22	0.77	0.48	0.05	1.07	0.11	0.09	0.09	0.09	0.20	0.52	0.18
Total	100.04	101.38	100.34	100.18	100.68	100.82	99.38	100.97	100.66	101.02	100.81	101.31	99.78	100.96	100.87	99.52
Cations (apfu)																
Si	2.19	2.18	2.21	2.25	2.33	2.24	2.26	2.21	2.27	2.19	2.19	2.19	2.21	1.91	1.91	2.68
Al	1.75	1.79	1.77	1.74	1.61	1.80	1.79	1.83	1.73	1.79	1.79	1.80	1.79	1.76	1.77	1.35
Ti	0.00	0.00	0.00	0.00	0.00	0.00	0.00	0.00	0.00	0.00	0.00	0.00	0.00	0.00	0.00	0.00
Fe	0.02	0.02	0.02	0.02	0.02	0.02	0.02	0.01	0.03	0.02	0.02	0.02	0.02	0.04	0.04	0.01
Mn	0.00	0.00	0.00	0.00	0.00	0.00	0.00	0.00	0.00	0.00	0.00	0.00	0.00	0.00	0.00	0.00
Mg	0.00	0.01	0.01	0.00	0.01	0.02	0.01	0.00	0.04	0.00	0.00	0.01	0.00	0.00	0.00	0.00
Ca	0.86	0.83	0.79	0.76	0.75	0.69	0.69	0.75	0.65	0.85	0.84	0.82	0.80	1.38	1.36	0.34
Na	0.14	0.13	0.15	0.19	0.25	0.13	0.14	0.14	0.22	0.12	0.12	0.12	0.12	0.21	0.21	0.46
K	0.01	0.01	0.01	0.01	0.01	0.04	0.03	0.00	0.06	0.01	0.01	0.00	0.01	0.02	0.01	0.01
Or	0.64	0.63	0.80	0.89	1.26	5.15	3.26	0.35	6.68	0.64	0.54	0.52	0.55	1.06	0.89	1.24
Ab	13.62	13.81	16.19	19.69	24.75	15.20	16.23	15.75	23.42	12.12	12.30	12.85	12.50	13.17	13.37	56.81
An	85.73	85.56	83.01	79.42	73.99	79.65	80.51	83.90	69.90	87.24	87.16	86.63	86.95	85.77	85.74	41.94

amphiboles are tremolite (Figure 5c). The Si content of magmatic amphibole is less than 7.4 apfu (Agemar et al., 1999). In this study, the amphiboles are magmatic, as indicated by the Si content of the studied samples. Ti, K, Na, and Al contents of calc-alkaline amphiboles are lower than those of alkaline amphiboles. Accordingly, the studied amphiboles are calc-alkaline. In this study, primary amphiboles are used to calculate temperature and pressure of amphibole crystallization.

4.3. Whole-rock geochemistry

Geochemical data of the 10 samples from the studied diabase dikes with minimum weathering are presented in Table 1.

The samples are positioned in the field of subalkaline basalt on the Zr/TiO_2 vs. Nb/Y diagram (Figure 6a) (Winchester and Floyd, 1977). On the K_2O vs. SiO_2 diagram (Le Maitre et al., 1989), samples plot within the calc-alkaline field (Figure 6b). The samples have high Al_2O_3 (16.65- 19.25) and moderately low Mg# (27.41-44.26), along with largely variable amounts of K_2O (0.6-1.04).

The pattern of primitive mantle-normalized incompatible trace elements is shown in Figure 6c (McDonough and Sun, 1995). The pattern shows enrichment in large ion lithophile elements (LILE; e.g., Sr, K, Rb Ba) and light rare earth elements (LREE; e.g., Ce) and depletion in high field strength elements (HFSE; e.g., Ta, Nb, Ti, Zr, Hf, and Y) and heavy rare earth elements (HREE; e.g., Yb). Rare earth elements (REEs), which are normalized to chondrite (Boynton, 1984), show significant enrichment in LREE (Figure 6d). REEs with generally sloping patterns show an enrichment in all REE, with

Table 4. Representative chemical composition and calculated mineral formulae of amphiboles from the JBG mafic dykes. Formulae calculated on the basis of 23 oxygens, Mg#=Mg/ (Fe^{2+}+Mg).

Samples	jb16	5jb16	pjb16	3p5jb16	4p5jb16	S2jb35	S3jb35	S2jb35	S32jb35	S4b35	
Oxides (wt%)											
SiO_2	43.12	42.61	43.61	43.52	43.22	40.88	41.33	41.36	41.50	40.96	
TiO_2	1.87	1.95	2.06	2.19	2.01	3.62	3.44	2.50	3.27	2.83	
Al_2O_3	13.09	12.99	11.15	11.78	12.53	13.11	13.10	12.60	12.23	12.01	
FeO	12.54	12.44	12.67	12.16	11.61	12.03	12.80	14.52	12.32	15.90	
MnO	0.24	0.22	0.17	0.14	0.18	0.09	0.17	0.24	0.26	0.22	
MgO	13.40	13.55	14.51	12.73	13.62	13.20	12.75	11.63	12.37	10.94	
CaO	11.40	11.63	12.31	11.82	11.84	11.67	11.46	11.64	11.72	12.15	
Na_2O	2.20	2.34	2.58	2.66	2.79	2.41	2.39	2.38	2.24	2.37	
K_2O	0.45	0.43	0.48	0.22	0.50	1.13	1.22	1.25	1.22	1.34	
Total	98.31	98.17	99.54	97.22	98.30	98.14	98.65	98.11	97.12	98.73	
(apfu) Cations											
Si	6.19	6.14	6.25	6.41	6.27	5.98	6.02	6.13	6.18	6.12	
Ti	0.20	0.21	0.22	0.24	0.22	0.40	0.38	0.28	0.37	0.32	
Al	2.21	2.21	1.88	2.04	2.14	2.26	2.25	2.20	2.15	2.11	
Al^{IV}	1.81	1.86	1.75	1.59	1.73	2.02	1.98	1.87	1.82	1.88	
Al^{VI}	0.40	0.35	0.14	0.45	0.41	0.24	0.27	0.32	0.32	0.23	
Fe	1.50	1.50	1.52	1.50	1.41	1.47	1.56	1.80	1.53	1.99	
Fe^{3+}	0.81	0.76	0.58	0.13	0.33	0.43	0.47	0.38	0.15	0.18	
Fe^{2+}	0.69	0.74	0.94	1.36	1.07	1.04	1.09	1.42	1.38	1.80	
Mn	0.03	0.03	0.02	0.02	0.02	0.01	0.02	0.03	0.03	0.03	
Mg	2.86	2.91	3.10	2.79	2.94	2.88	2.77	2.57	2.74	2.44	
Ca	1.75	1.80	1.89	1.86	1.84	1.83	1.79	1.85	1.87	1.94	
Na	0.61	0.65	0.72	0.76	0.78	0.68	0.68	0.68	0.65	0.69	
K	0.08	0.08	0.09	0.04	0.09	0.21	0.23	0.24	0.23	0.25	
B: Ca	1.75	1.80	1.82	1.74	1.76	1.83	1.76	1.85	1.81	1.89	
B: Na	0.25	0.20	0.18	0.26	0.24	0.17	0.24	0.15	0.19	0.11	
Mg#	0.66	0.66	0.67	0.65	0.68	0.66	0.64	0.59	0.64	0.55	
Oxides (wt%)											
SiO_2	41.89	42	42.39	41.48	41.9	41.55	42.09	44.43	46.04	51.55	45.72
TiO_2	3.72	3.05	2.45	3.67	3.78	3.67	3.68	2	1.75	0	1.65
Al_2O_3	11.75	12.48	13.23	13.95	11.49	12.67	12.56	10.71	9.73	4.42	10.29
FeO	12.05	12.64	12.03	11.6	12.07	11.98	11.71	14.28	13.85	12.66	16.51
MnO	0.14	0.2	0.18	0.12	0.16	0.12	0.1	0.39	0.53	0.59	0.42
MgO	13.21	12.5	13.54	11.81	13.96	13.61	13.02	12.47	13.07	14.73	12.56
CaO	12.01	12.03	11.53	12.15	11.16	11.44	11.81	11.71	10.29	12.67	10.22
Na_2O	2.49	2.27	2.32	2.06	2.33	2.39	2.35	1.72	2.3	0.33	2.14
K_2O	1.26	1.23	1.09	1.19	1.2	1.27	1.29	1.06	0.26	0.14	0.37
Total	98.52	98.4	98.75	98.04	98.05	98.68	98.61	98.77	97.83	97.09	99.87

Table 4. Continued.

(apfu) Cations											
Si	6.16	6.18	6.11	6.12	6.1	6.03	6.15	6.46	6.63	7.46	6.46
Ti	0.41	0.34	0.27	0.41	0.41	0.4	0.4	0.22	0.19	0	0.18
Al	2.04	2.16	2.25	2.43	1.97	2.17	2.16	1.84	1.65	0.75	1.71
Al^{IV}	1.84	1.82	1.89	1.88	1.9	1.97	1.85	0	1.37	0.54	1.54
Al^{VI}	0.19	0.34	0.36	0.54	0.07	0.19	0.32	4.82	0.28	0.21	0.18
Fe	1.48	1.55	1.45	1.43	1.47	1.45	1.43	1.74	1.67	1.53	1.95
Fe^{3+}	0.09	0.13	0.6	0	0.64	0.52	0.12	0.48	0.86	0.28	1.26
Fe^{2+}	1.39	1.42	0.85	1.43	0.83	0.93	1.31	1.26	0.81	1.26	0.69
Mn	0.02	0.02	0.02	0.02	0.02	0.01	0.01	0.05	0.06	0.07	0.05
Mg	2.89	2.74	2.91	2.6	3.03	2.94	2.84	2.7	2.8	3.18	2.65
Ca	1.89	1.9	1.78	1.92	1.74	1.78	1.85	1.82	1.59	1.96	1.55
Na	0.71	0.65	0.65	0.59	0.66	0.67	0.67	0.48	0.64	0.09	0.59
K	0.24	0.23	0.2	0.22	0.22	0.23	0.24	0.2	0.05	0.03	0.07
B: Ca	1.81	1.84	1.77	1.86	1.85	1.75	1.8	1.79	1.53	1.92	1.55
B: Na	0.19	0.16	0.23	0.14	0.15	0.25	0.2	0.21	0.47	0.08	0.45
Mg#	0.66	0.64	0.67	0.64	0.67	0.67	0.66	0.61	0.63	0.67	0.58

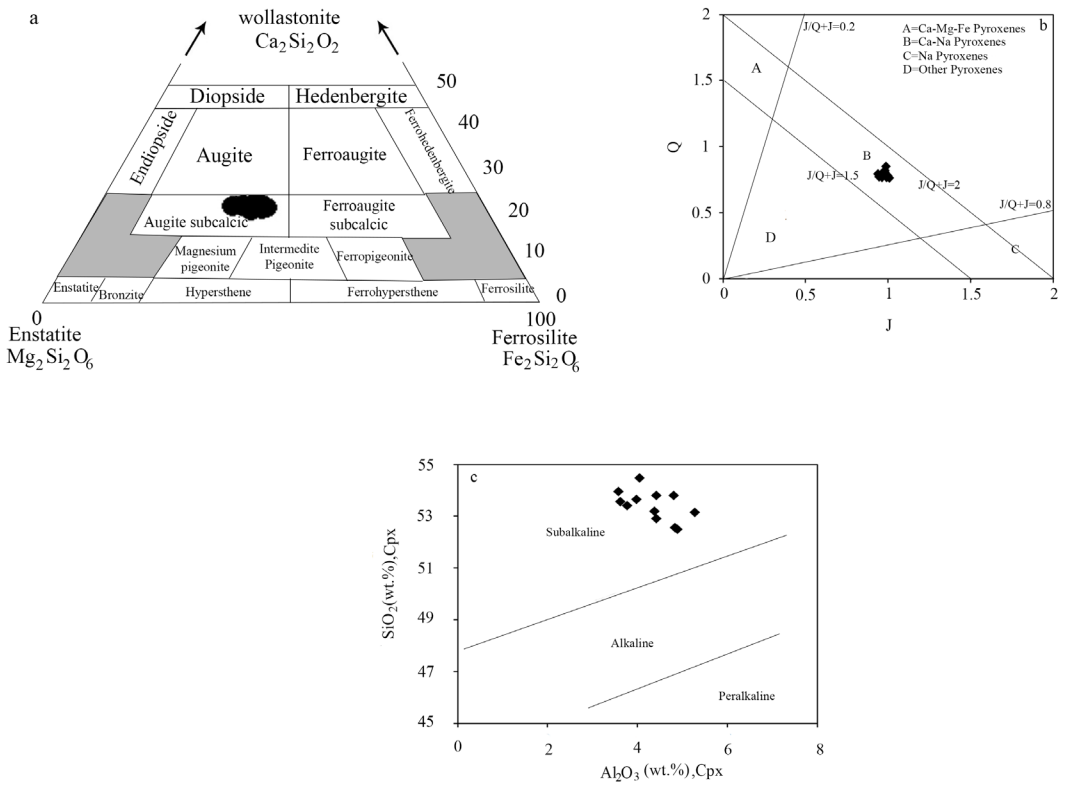

Figure 4. Classification and discriminant diagrams for clinopyroxene (after Morimoto, 1988) of the studied mafic dikes: (a) En–Wo–Fs ($Mg_2Si_2O_6$–$Ca_2Si_2O_6$–$Fe_2Si_2O_6$) plot, (b) Q-J (Q=Ca+Mg+Fe^{2+}, J=2Na) plot and (c) SiO_2–Al_2O_3 plot.

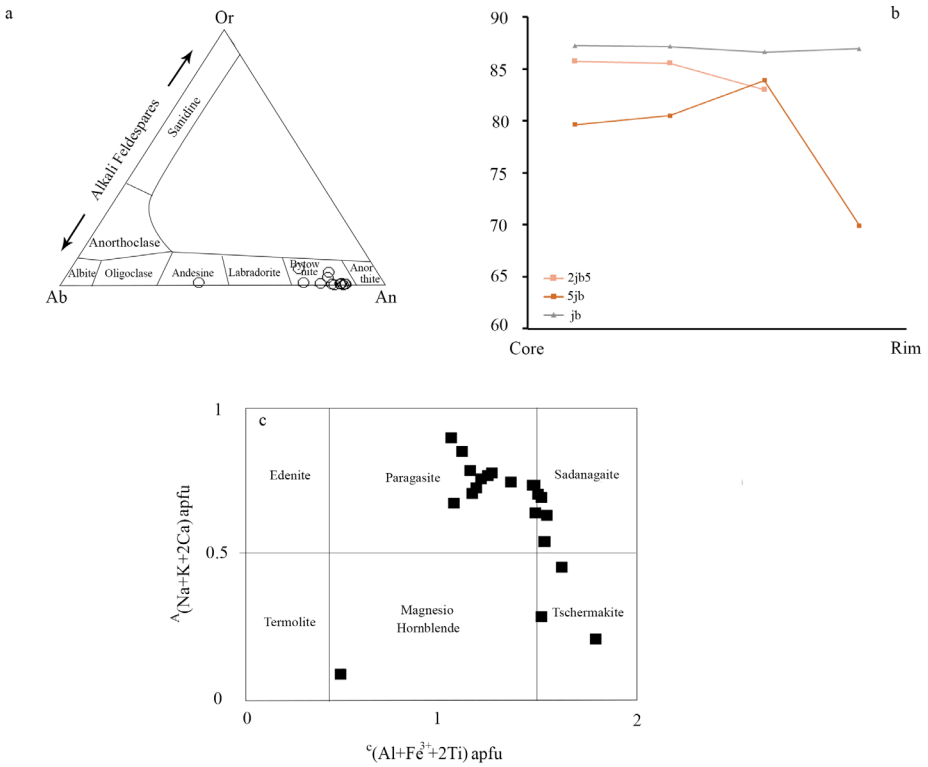

Figure 5. (a) Classification ternary diagram for feldspar (Ab–An–Or plot; Deer et al., 1992), (b) Variation diagram for plagioclase and (c) Classification diagram (Hawthorne et al., 2012) for amphibole of the studied mafic dikes.

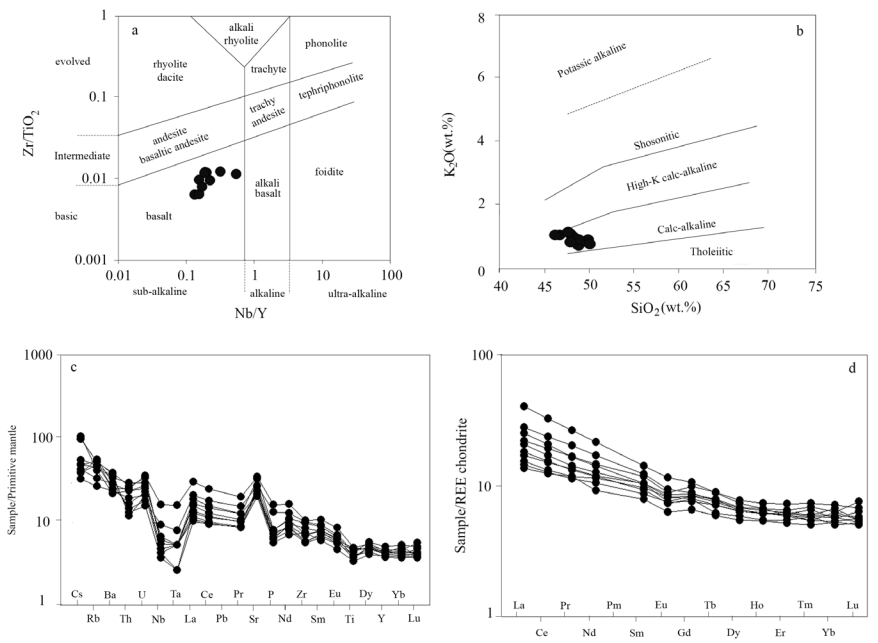

Figure 6. (a) Zr/TiO_2–Nb/Y classification diagram (Winchester and Floyd, 1977), (b) K_2O–SiO_2 classification diagram (Le Maitre et al., 1989), (c) Primitive mantle-normalized multielement patterns (McDonough and Sun, 1995), and (d) REE-normalized patterns (Boynton, 1984) for the JBG mafic dikes.

higher enrichment of LREE than HREE (La/Yb = 3.2–10). Eu shows weak negative anomaly (Eu/Eu^{*} = 0.81–0.92).

5. Discussion

5.1. Tectonic setting

The studied dikes and the host granitic rocks are a part of the UDMA. The UDMA has a complex geological history involving the formation of voluminous volcanic rocks from Eocene to Quaternary (Agard et al., 2011; Shahabpour, 2005), intrusion of igneous bodies into previous rocks from late Eocene to the Miocene (Dimitrijevic, 1973; Shafiei et al., 2009), and also collision and postcollision related events (Allen et al., 2013; Ghasemi and Talbot, 2006). Many authors think that this magmatic arc developed along an active continental margin (e.g., Berberian et al., 1982; Ghorbani et al., 2014; Rasouli et al., 2014) and formed due to subduction of Neotethyan lithosphere beneath the Central Iran zone (Aftabi and Atapour, 2000; Berberian and Berberian, 1981).

In order to identify the tectonic setting of the studied rocks, major and trace elements should be considered. Based on the Nb/Th-Y diagram (Swinden et al., 1989), all the samples plot within the arc field (Figure 7a). High Sr contents of the samples confirm their arc character (Figure 6c). On the Zr/Y vs. Zr diagram (Pearce, 1982), which distinguishes between continental arc and oceanic arc environments, all of the samples plot in the continental arc area (Figure 7b). On the Th vs. Hf vs. Nb discrimination diagram (Wood, 1980), all the samples plot in the supra-subduction zone (SSZ) field (Figure 7c). The Zr/Y rate affinities provide additional information about the tectonic environment. Accordingly, if Zr/Y > 3, the volcanic rocks are likely to form in a continental volcanic arc, and Zr/Y < 3 infers that the volcanic rocks formed in an oceanic volcanic arc (Pearce and Norry, 1979). With Zr/Y rate of the samples being higher than 3 (3.25–5.73), the samples are described as from a continental volcanic arc. According to Ba/Nb > 32, the studied samples exhibit characteristics of arc magma (Fitton et al., 1988). With Ba/La >15 and La/Th <7, the samples resemble active continental margin rocks (Gill, 1981).

The Na vs. Cr diagram (Kornprobst et al., 1981) shows the clinopyroxenes from the diabase dikes formed in a continental environment (Figure 7d). In Nisbet and Pearce's (1977) diagram, the studied clinopyroxenes plotted in the volcanic arc field (Figure 7e). Using the SiO_2 vs. Na_2O diagram (Coltorti et al., 2007) for amphiboles (Figure 7f), it can be deduced that a subduction zone is the origin of amphiboles in the diabase dikes. In order to separate different tectonic environments, a threshold of Al^{IV} = 1.5 was considered. Accordingly, the Al^{IV} value of high-pressure amphiboles (~10 kbar) formed in magmatic arcs is higher than 1.5 (Jiang and An, 1984). Based on the Al^{IV} value, the studied amphiboles (Al^{IV} > 1.5) formed in a magmatic arc zone. Thus, mineral chemistry results are in agreement with those of whole-rock geochemistry studies inferring a volcanic arc setting for the studied rocks.

5.2. Fractional crystallization

Crystallization of mafic minerals from primitive melts at high pressure results in high concentration of Al_2O_3 in the basalts (Gust and Perfit, 1987). The Al_2O_3 is concentrated in the remaining melt and plagioclase crystallizes at lower pressure. The content of Al_2O_3 in the intermediate orogeny rocks was estimated as 16–18 wt.% (Gill, 1981). According to Al_2O_3 contents of the studied rocks, the samples are found to be metaluminous and orogenic rock type. The lack of negative correlation between P_2O_5, TiO_2 and MgO can be explained by fractionation of accessory minerals such as apatite and Fe-Ti oxide (Kampunzu and Lubala, 2012) (Table 1). Low MgO (<6 wt.%), Mg# (27.41–44.26 wt.%), Cr (10–360 ppm) and Ni (5–123 ppm) indicate that the magma in the dikes is not primary (Wilson, 1989), i.e. the studied dikes originated from a primary magma subsequently affected by fractional crystallization. This understanding is further supported by the presence of pyroxene and plagioclase and positive correlations between MgO, Al_2O_3, CaO, K_2O, Sr, and Cr. High Sr contents, along with the lack of Eu anomalies, suggest absence of plagioclase crystal fractionation (Figure 6d).

5.3. Geothermobarometry estimations

Crystallization temperature and pressure of pyroxene and amphibole can be estimated from their chemical composition, helping to understand the physical conditions of crystallization.

Aluminum distribution in tetrahedral and octahedral sites of clinopyroxene can be used as a standard for estimating environmental pressure of pyroxene formation in igneous rocks (Helz, 1973). Given that Al^{VI} is a function of formation pressure (Aoki and Shiba, 1973), the Al^{VI} vs. Al^{IV} diagram (Figure 8a) shows the pressure fields defined by Aoki and Kushiro (1968). Accordingly, the samples fall above the Al^{VI}/Al^{IV} = 0.25 line (Figure 8a). Since this line represents a pyroxene crystallization pressure of 5 kbar, the studied clinopyroxenes crystallized at some pressure above 5 kbar (Helz, 1973). Another method for calculating geothermobarometry of clinopyroxene was proposed by Soesoo (1997), based on crystallization pressure and temperature of the studied clinopyroxenes from 2 to 5 kbar (Figure 8b) and 1100 to 1150 °C (Figure 8c), respectively. Estimated values of clinopyroxene crystallization temperature and pressure using various methods are shown in Table 5. The clinopyroxene pressure (Putirka, 2008) vs. mg# diagram is graphically represented. According to

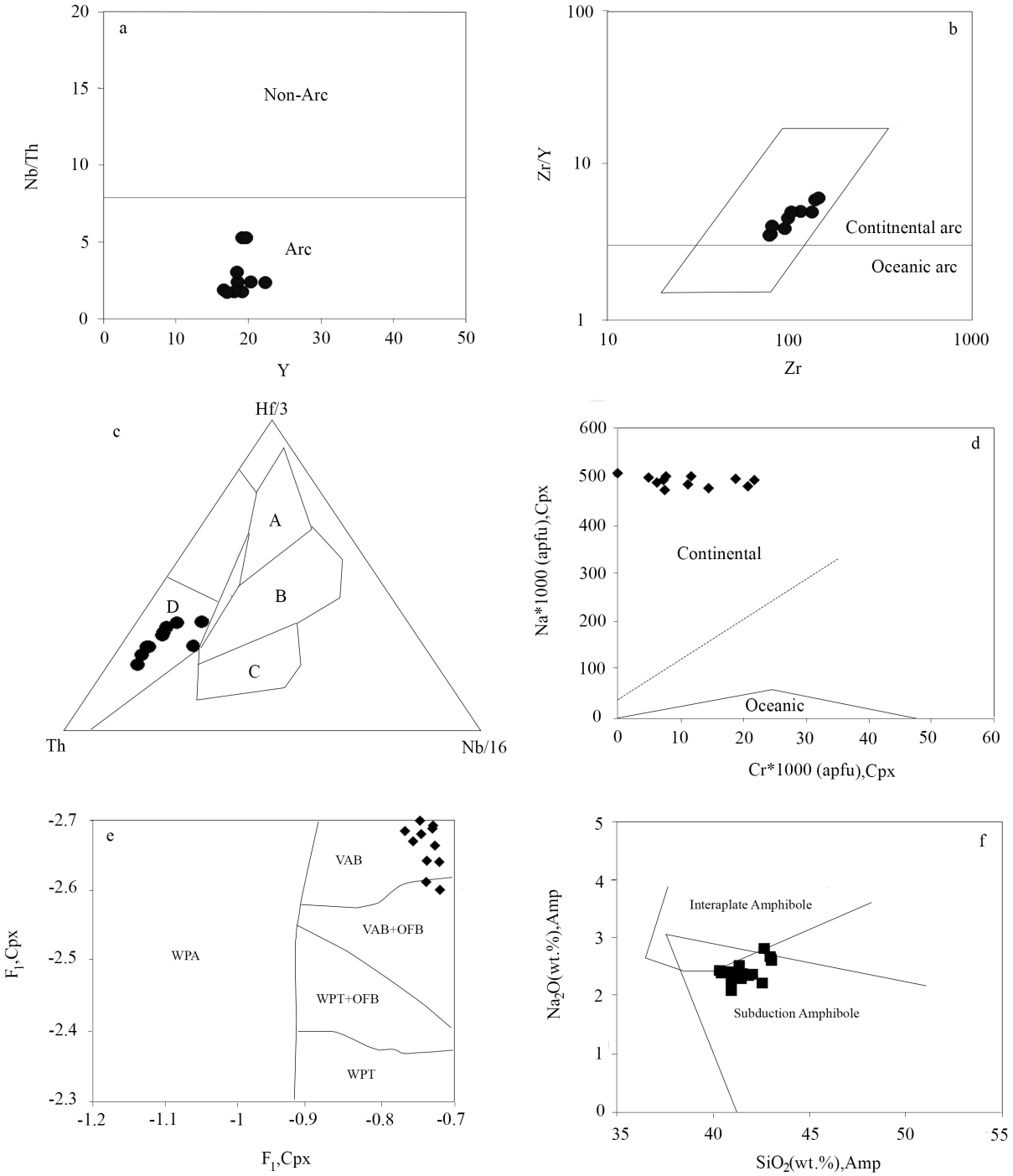

Figure 7. Tectonic setting discrimination diagrams based on whole-rock chemical compositions for the JBG mafic dikes: (a) Nb/Th–Y diagram (Swinden et al., 1989), (b) Zr– Zr/Y diagram (Pearce, 1982), (c) Th–Hf–Nb diagram (Wood, 1980). A - normal mid-ocean ridge basalts (N-MORB); B - enriched mid-ocean ridge basalts (E-MORB) and tholeiitic basalts within plate and differentiates; C - alkaline within plate basalts and within plate basalts and differentiates; D - destructive plate-margin basalts and differentiates (subduction zone). Tectonic setting determination diagrams based on mineral chemical data of the studied mafic dikes minerals: (d) Cr–Na diagram (Kornprobst et al., 1981), e) F_1 - F_2 (Nisbet and Pearce, 1977) and, (f) SiO_2–Na_2O diagram (Coltorti et al., 2007) [F1 = - (0.012 * SiO_2) – (0.0807 * TiO_2) + (0.0026 * Al_2O_3) – (0.0012 * FeO^t) – (0.0026 * MnO) + (0.0087 * MgO) – (0.0128 * CaO) – (0.0419 * Na_2O) , F2 =- (0.0469 * SiO_2) – (0.0818 * TiO_2) + (0.0212 * Al_2O_3) – (0.0041 * FeO^t) – (0.1435 * MnO) + (0.0029 * MgO) – (0.0085 * CaO) – (0.016 * Na_2O)].

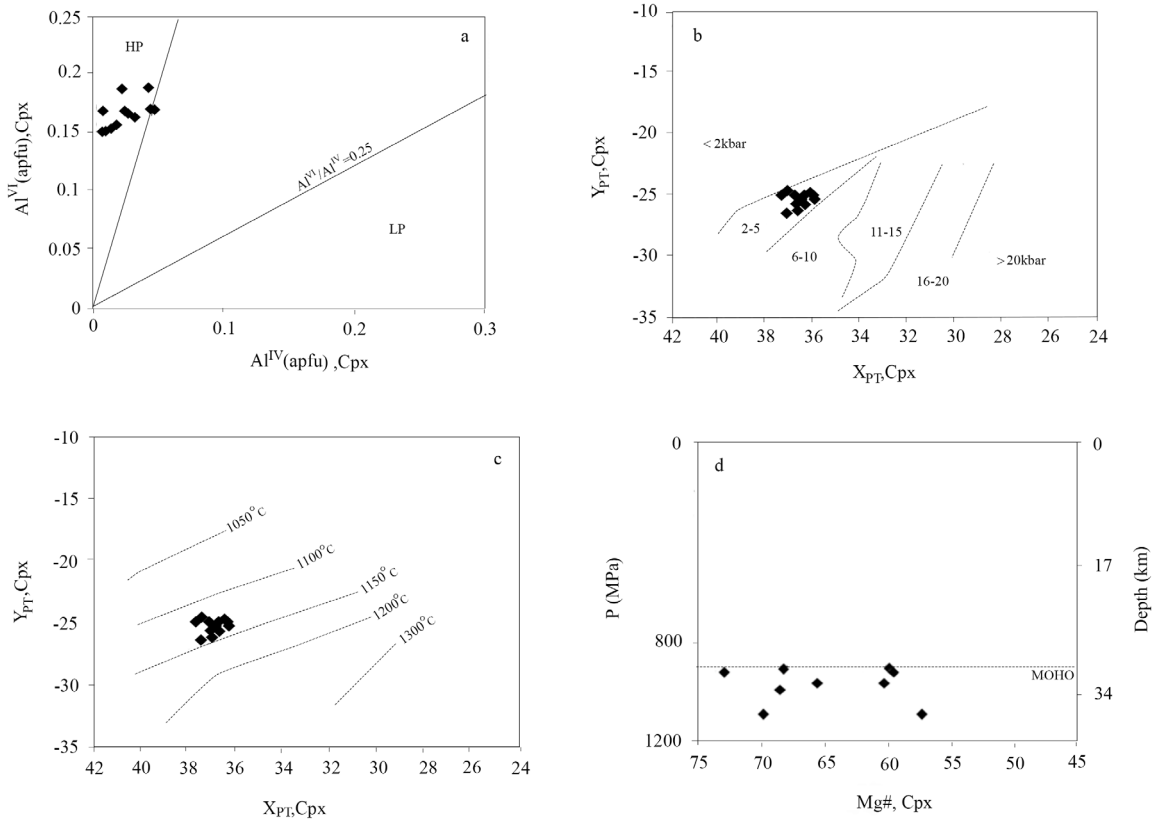

Figure 8. Clinopyroxene thermobarometry of the JBG mafic dikes: (a) Al^{VI}–Al^{IV} diagram (Aoki and Kushiro, 1968) [HP: High Pressure, LP= Low Pressure], (b and c) X_{PT}–Y_{PT} diagram (Soesoo, 1997) [X_{PT}= (0.446 * SiO_2) + (0.187 * TiO_2) - (0.404 * Al_2O_3) + (0.346 * FeO^t) - (0.052 * MnO) + (0.309 * MgO) + (0.431 * CaO) - (0.446 * Na_2O), Y_{PT} = (-0.369 * SiO_2) + (0.535 * TiO_2) - (0.317 * Al_2O_3) + (0.323 * FeO^t) + (0.235 * MnO) - (0.516 * MgO) - (0.167 * CaO) - (0.153 * Na_2O)], (d) Pressure estimates according to equation 32b by Putirka (2008) vs. Mg# content, the vertical right axis shows the equivalence of pressure in depth.

continental crust density (3 g/cm), equivalence in depth of pressure values is shown in this diagram (Figure 8d).

This barometric data is useful for determining petrogenetic information about various stages of the magmatic history. The studied clinopyroxene composition is in agreement with a fractionation process in a magma chamber located at the mantle-crust transition or lower crust. The crystallization level at a depth of 30–40 km could indicate a probable magma chamber where these crystals had enough time to grow to large size (Figure 8d).

The Al^{VI} value of amphibole depends on temperature, which is affected in turn by water content of magma (Jiang et al., 1984). Using Al^{VI} and Al^t values of amphibole, the pressure is estimated based on amphibole composition (Blundy and Holland, 1990; Vynhal et al., 1991; Schmidt, 1992). According to Schmidt (1992), average amphibole crystallization pressure is 6.51 kbar. The amphibole crystallization temperature can be estimated using amphibole-plagioclase couples. Considering Schmidt's (1992) average pressure and the latter method, average crystallization temperature of the studied amphibole is 1064 °C. Table 6 shows estimated temperature and pressure of amphibole crystallization based on various methods.

5.4. Crustal contamination evidence

During dike emplacement into crustal levels, different degrees of crustal contamination occur in mantle-derived magmas (Mohr, 1987). The crustal contamination can be determined by checking the correlations between trace elements of the mantle and crust. For example, in continental crust, the values of Ce/Pb and Ba/Nb ratios are 3.9 and 57, respectively (Rudnick and Gao, 2003). Given that the Ba/Nb ratio of the studied samples are 57.57, the basaltic magma is found to be contaminated by crustal components. Furthermore, elevated abundances of Rb, U, and Pb and depletion of Nb, Ta, and Ti are indicative of crustal contamination of the samples (Figure 6c) (Rudnick

Table 5. Estimation of crystallization geothermobarometry of studied clinopyroxenes

Methods			
	P (kbar)		
	Min	Max	Average
Putirka (1996)	6.9	10.5	9.03
Putirka et al. (2003)	7.1	10.8	9.72
Putirka, 2008 (equation 32b)	8.9	12.2	10.72
Nimis (1999)	5.3	9.2	7.33
	T (°C)		
Putirka (1996)	1242	1284	1271
Putirka et al. (2003)	1267	1312	1294
Putirka, 2008 (equation 32b)	1182	1210	1200
Nimis and Taylor (2000)	1197	1225	1208
Kretz (1994)	1205	1234	1218

Table 6. Estimation of crystallization geothermobarometry of studied amphiboles.

Methods			
	P (kbar)		
By Al in amphibole	Min	Max	Average
Hammarstrom and Zen (1986)	6.32	8.28	7.07
Hollister (1987)	5.24	5.55	5.25
Johnson and Rutherford (1989)	5.84	6.70	6.23
Schmidt (1992)	6.72	8.53	6.51
Anderson and Smith (1995)	5.93	7.05	5.64
	T (°C)		
Otten (1984)	800	985	872
Colombi (1989)	797	993	867
By amphibole-plagioclase			
Holland and Blundy (1994)	984	1097	1064

and Gao, 2003). Moreover, the incompatible element ratios such as Nb/Th, Ce/Yb, and Zr/Y could be used to determine crustal contamination where Nb/Th and Ta/U ratios are known to capture the source characteristics and remain constant during basaltic magmatism (Pearce and Norry, 1979). In that respect, Nb/Th and Ta/U ratios decrease with increasing SiO_2 when mafic magmas are contaminated by the crust (Hu et al., 2016) (Figure 9a, 9b). Additionally, the Ce/Yb vs. Zr/Y diagram (Weaver and Tarney, 1984) shows the possibility of crustal contamination for the studied rocks (Figure 9c).

Fractional crystallization and crustal contamination play important roles in magma evolution and can change elemental compositions (DePaolo, 1981). Mafic dikes have relatively higher SiO_2 (46.8–50.2 wt.%) along with lower MgO (3.78–8.34 wt.%), Ni (5–45 ppm) and Mg# (0.27–0.44) compared to basaltic rocks, which is indicative of their highly evolved nature from mantle-derived parental melts through fractional crystallization of clinopyroxene and crustal contamination.

The Lu/Yb ratio of the mantle-derived magma is low (0.14–0.15) (Sun and McDonough, 1989), while continental crust exhibits relatively higher values of Lu/Yb ratio (0.16–0.18). The relatively high Lu/Yb ratios of the samples (0.14–0.18) are indicative of crustal contamination during magmatic evolution; in fact, the depletion in Nb and Ta confirms crustal contamination in magma (Figure 6c). Crustal components are rich in Zr, Hf, and Th and depleted in Nb and Ta (Rudnick and Gao, 2003), as the mantle-derived melt is depleted in Nb-Ta-Ti during subduction-zone magmatism and crustal contamination, thus resulting in negative Nb-Ta and positive Zr-Hf anomalies in the spider diagram for mantle-derived melts (Figure 6c).

5.5. Origin of the studied dikes

Different mineralogical and geochemical characteristics along with related diagrams can be used to distinguish the nature of the source and genesis of the studied dikes. For example, as illustrated in Figure 10a (Jiang and An, 1984), amphiboles from the dikes fall in the mantle-derived amphibole field. Mafic magmas, which formed in the arc environment, are derived from mantle wedges and are later modified by slab-derived hydrous fluids (Kimura and Yoshida, 2006). LREE/HFSE and LILE/HFSE ratios of the arc magmas with slab melt-modified mantle origins are lower than those of magmas with fluid-modified mantle origins (Ayers, 1998; Class et al., 2000). The studied mafic dikes exhibit high Zr/Nb (17.41–25), low Th/U (2.25–4) and moderate Nb/Ta ratios (14.5–25), resembling the basalts/diabase from island arcs (Münker, 1998). The low La/Sm (2.24–3.1), Nb/Zr (0.04–0.09), and Th/Zr ratios (0.001–0.003) of the studied diabases reveal the mantle source was modified by slab fluids (Figure 10b).

The nature of the mantle source can be determined by the contents of HREEs in magma and garnet partition coefficient (Jenner et al., 1993). The high values of Sm/Yb (>5) and La/Yb ratios (>20) indicate that large quantities of HREEs remained in the garnet and amphibole of the source (Kay et al., 1994; Haschke and Gunther, 2003). According to Sm/Yb and La/Yb ratios (1.35–2.30, 3.23–6/17; respectively), the mantle source is garnet-free. The diagram of Sm/Yb vs. Ce/Sm (Çoban, 2007) shows partial

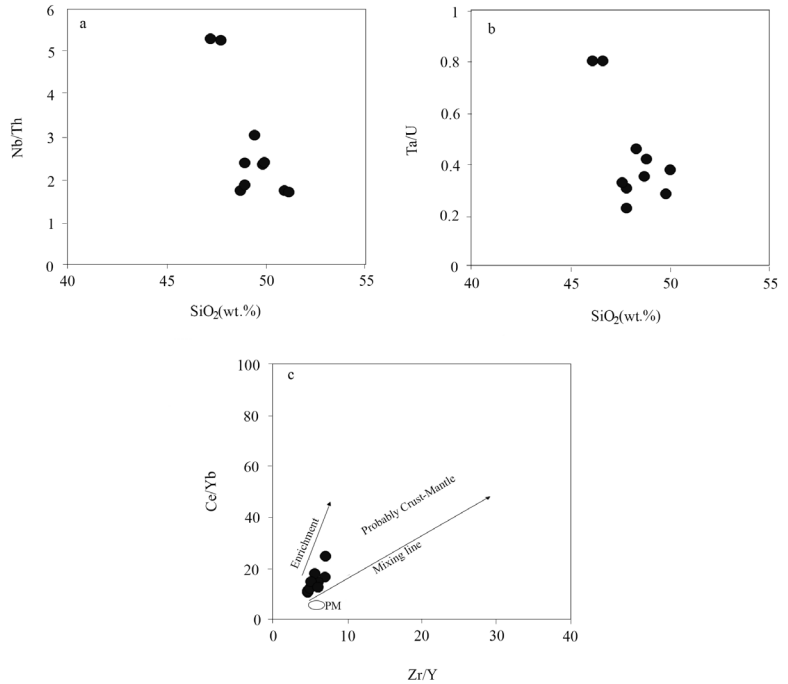

Figure 9. (a) Nb/Th–SiO_2 and (b) Ta/U–SiO_2 diagrams (Hu et al., 2016) of the JBG mafic dikes. The weak negative Nb/Th and Ta/U correlations with SiO_2 are consistent with crustal contamination during magma ascent. (c) Zr/Y–Ce/Yb diagram (Weaver and Tarney, 1984) for the studied mafic dikes.

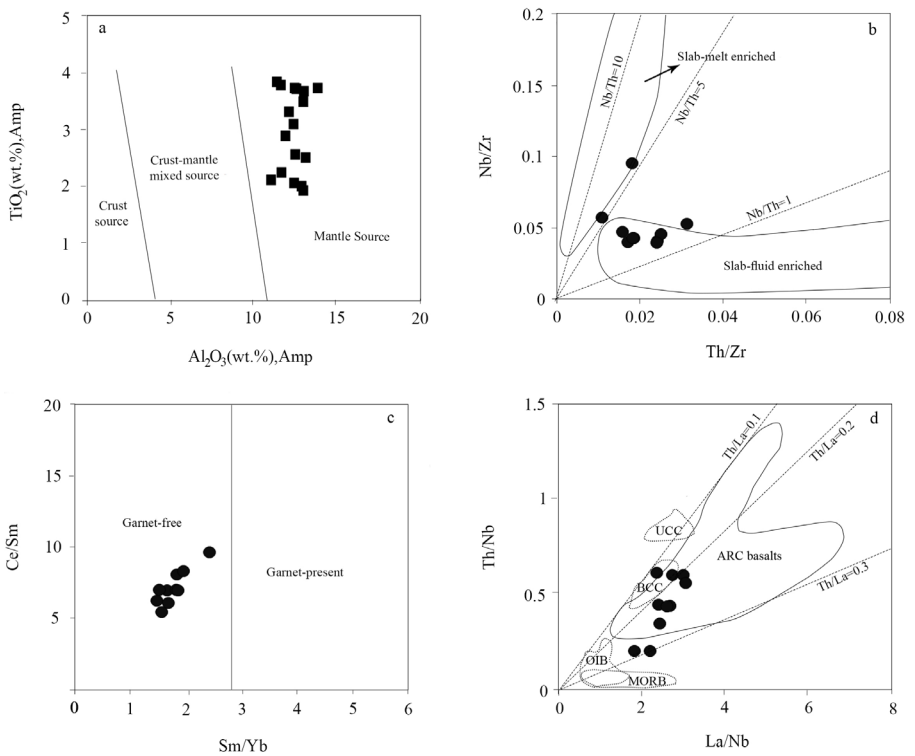

Figure 10. (a) Al_2O_3–TiO_2 diagram (Jiang and An, 1984), (b) Nb/Zr–Th/Zr diagram, (c) Ce/Sm–Sm/Yb diagram (Çoban, 2007), and (d) La/Nb–Th/Nb diagram (Plank, 2005) for the studied mafic dikes, UCC: average upper continental crust, BCC: average bulk continental crust.

melting process from a garnet-free mantle source (Figure 10c).

Given the presence of trace elements (Figure 6c), the primitive magmas from which these mafic dikes are sourced, were derived from mantle sources enriched in incompatible elements at higher rates than those of OIB sources (Figure 10d). Although melting of subcontinental lithospheric mantle metasomatized in a mantle wedge environment could produce primary and parental magma for the mafic dikes (Zhao et al., 2009). In Figure 9c, studied samples follow the enrichment trend, which is probably enriched by mantle metasomatism (Ahmad and Tarney, 1993). The Th/Nb-La/Nb ratios of all the studied samples are similar to those of arc basalt (Plank, 2005), indicating evolution by crustal components or melting of metasomatized mantle lithosphere with possible sediment input (Figure 10d).

6. Conclusions

1- The studied mafic dikes (diabases) trend N50–70W and N20–40W intruded into the Oligo-Miocene Jebal-E-Barez granitoids.

2- Small abundances of MgO, Ni and Mg# suggest that the parent magma underwent crystal fractionation of clinopyroxene and plagioclase.

3- The estimations of crystallization pressures and temperatures based on clinopyroxenes from the studied mafic dikes show ~8 kbar and ~1100 °C, respectively. According to this pressure, the crystallization levels were located at depths of 30–40 km and indicate it was probably a magma chamber placed at the mantle-crust transition or lower crust.

4- Mineral chemistry and whole-rock geochemistry data are consistent with generation of the primitive melts by partial melting of a garnet-free mantle source. The La_N/Sm_N and La_N/Lu_N ratios indicate the magma was generated from an enriched mantle source, but the parental magmas were further evolved by crustal components.

5- All evidence shows that the studied mafic dikes formed in an active continental arc environment.

Acknowledgments

This research forms part of the PhD study of the first author which was financially supported by the Shahid Bahonar University of Kerman. The authors sincerely wish to thank the journal editor and reviewers who critically reviewed the manuscript and made valuable suggestions for its improvement.

References

Aftabi A, Atapour H (2000). Regional aspects of shoshonitic volcanism in Iran. Episodes 23: 119-125.

Agard P, Omrani J, Jolivet L, Whitechurch H, Vrielynck B et al. (2011). Zagros orogeny: a subduction-dominated process. Geological Magazine 148: 692-725.

Agemar T, Wörner G, Heumann A (1999). Stable isotopes and amphibole chemistry on hydrothermally altered granitoids in the North Chilean Precordillera: a limited role for meteoric water?. Contributions to Mineralogy and Petrology 136: 331-344.

Ahmad T, Tarney J (1993). North Indian Proterozoic volcanics, products of lithosphere extension: Geochemical studies bearing on the lithospheric derivation rather than crustal contamination. In: Casshyap SM, editor. Rifted basins and aulacogens, geological and geophysical approach. Gyanodaya Prakashan Nainitial, India 130-147.

Allahyari K, Saccani E, Pourmoafi M, Beccaluva L, Masoudi F (2010). Petrology of mantle peridotites and intrusive mafic rocks from the Kermanshah ophiolitic complex (Zagros belt, Iran): implications for the geodynamic evolution of the Neo-Tethyan oceanic branch between Arabia and Iran. Ofioliti 35: 71-90.

Allen M, Kheirkhah M, Neill I, Emami M, McLeod C (2013). Generation of arc and within-plate chemical signatures in collision zone magmatism: Quaternary lavas from Kurdistan Province, Iran. Journal of Petrology 54: 887-911.

Anderson JL, Smith DR (1995). The effects of temperature and fO_2 on the Al-in-hornblende barometer. American Mineralogist 80: 549-559.

Aoki KI, Kushiro I (1968). Some clinopyroxenes from ultramafic inclusions in Dreiser Weiher, Eifel. Contributions to Mineralogy and Petrology 18: 326-337.

Aoki KI, Shiba I (1973). Pyroxenes from lherzolite inclusions of Itinome-gata, Japan. Lithos 6: 41-51.

Arvin M, Robinson PT (1994). The petrogenesis and tectonic setting of lavas from the Baft ophiolitic mélange, southwest of Kerman, Iran. Canadian Journal of Earth Sciences 31: 824-834.

Ayers J (1998). Trace element modeling of aqueous fluid–peridotite interaction in the mantle wedge of subduction zones. Contributions to Mineralogy and Petrology 132: 390-404.

Bagheri S, Stampfli GM (2008). The Anarak, Jandaq and Posht-e-Badam metamorphic complexes in central Iran: new geological data, relationships and tectonic implications. Tectonophysics 451: 123-155.

Bayat F, Torabi G (2011). Alkaline lamprophyric province of Central Iran. Island Arc: 20, 386-400.

Berberian F, Berberian M (1981). Tectono-plutonic episodes in Iran. Zagros Hindu Kush Himalaya Geodynamic Evolution: 5-32

Berberian M, King G (1981). Towards a paleogeography and tectonic evolution of Iran. Canadian Journal of Earth Sciences 18: 210-265.

Berberian F, Muir I, Pankhurst R, Berberian M (1982). Late Cretaceous and early Miocene Andean-type plutonic activity in northern Makran and Central Iran. Journal of the Geological Society 139: 605-614.

Blundy JD, Holland TJ (1990). Calcic amphibole equilibria and a new amphibole-plagioclase geothermometer. Contributions to Mineralogy and Petrology 104: 208-224.

Bottinga Y, Kudo A, Weill D (1966). some observations on oscillatory zoning and crystallization of magmatic plagioclase. American Mineralogist 51: p. 792.

Boynton WV (1984). Geochemistry of the rare earth elements: meteorite studies. Rare Earth Element Geochemistry 63-114.

Buchan KL, Ernst R, Hanski E, Mertanen S, Rämö T, Vuollo J (2006). Giant dyke swarms and the reconstruction of the Canadian Arctic islands, Greenland, Svalbard and Franz Josef Land. Dyke swarms: time markers of crustal evolution 27-48.

Castro A, Aghazadeh M, Badrzadeh Z, Chichorro M (2013). Late Eocene–Oligocene post-collisional monzonitic intrusions from the Alborz magmatic belt, NW Iran. An example of monzonite magma generation from a metasomatized mantle source. Lithos 180: 109-127.

Class C, Miller DM, Goldstein SL, Langmuir CH (2000). Distinguishing melt and fluid subduction components in Umnak Volcanics, Aleutian Arc. Geochemistry, Geophysics, Geosystems Vol. 1.

Çoban H (2007). Basalt magma genesis and fractionation in collision-and extension-related provinces: A comparison between eastern, central and western Anatolia. Earth-Science Reviews 80: 219-238.

Colombi A (1989). Métamorphisme et géochimie des roches mafiques des Alpes ouest-centrales: (géoprofil Viège-Domodossola-Locarno). Université de Lausanne Faculté des sciences Institut de minéralogie et pétrographie (In French).

Coltorti M, Bonadiman C, Faccini B, Grégoire M, O'Reilly SY, Powell W (2007). Amphiboles from suprasubduction and intraplate lithospheric mantle. Lithos 99: 68-84.

Deer WA, Howie RA, Zussman J (1992). An Introduction to the Rock-forming Minerals. London, UK: Longman Scientific and Technical.

Depaolo DJ (1981). A neodymium and strontium isotopic study of the Mesozoic calc-alkaline granitic batholiths of the Sierra Nevada and Peninsular Ranges, California. Journal of Geophysical Research: Solid Earth 86: 10470-10488.

Dimitrijevic M (1973). Geology of Kerman region: institute for geological and mining exploration and investigation of nuclear and other mineral raw material, Beograd—Yugoslavia. Iran Geol, Survey Rept Yu/52.

Fitton J, James D, Kempton P, Ormerod D, Leeman W (1988). The role of lithospheric mantle in the generation of late Cenozoic basic magmas in the western United States. Journal of Petrology 1: 331-349.

Ghasemi A, Talbot C (2006). A new tectonic scenario for the Sanandaj–Sirjan Zone (Iran). Journal of Asian Earth Sciences 26: 683-693.

Ghorbani MR, Graham, IT, Ghaderi, M (2014). Oligocene–Miocene geodynamic evolution of the central part of Urumieh-Dokhtar Arc of Iran. International Geology Review 56: 1039-1050.

Gill JB (1981). What is "Typical Calcalkaline Andesite"? Orogenic Andesites and Plate Tectonics. Springer 1-12.

Gorring ML, Kay SM (2001). Mantle processes and sources of Neogene slab window magmas from southern Patagonia, Argentina. Journal of Petrology 42: 1067-1094.

Gust D, Perfit MR (1987). Phase relations of a high-Mg basalt from the Aleutian island arc: implications for primary island arc basalts and high-Al basalts. Contributions to Mineralogy and Petrology 97: 7-18.

Hammarstrom JM, Zen EA (1986). Aluminum in hornblende: an empirical igneous geobarometer. American Mineralogist 71: 1297-1313.

Haschke M, Gunther A (2003). Balancing crustal thickening in arcs by tectonic vs. magmatic means. Geology 31: 933-936.

Hawthorne FC, Oberti R, Harlow GE, Maresch WV, Martin RF et al. (2012). Nomenclature of the amphibole supergroup. American Mineralogist 97: 2031-2048.

Helz RT (1973). Phase Relations of Basalts in their Melting Range at PH_2O= 5 kb as a Function of Oxygen Fugacity 1: Part I. Mafic Phases. Journal of Petrology 14: 249-302.

Hoek J, Seitz HM (1995). Continental mafic dyke swarms as tectonic indicators: an example from the Vestfold Hills. East Antarctica, Precambrian Research 75: 121-139.

Holland T, Blundy J (1994). Non-ideal interactions in calcic amphiboles and their bearing on amphibole-plagioclase thermometry. Contributions to Mineralogy and Petrology 116: 433-447.

Hollister LS (1987). Confirmation of the empirical correlation of Al in hornblende with pressure of solidification of calc-alkaline plutons. American Mineralogist 72: 231-239.

Hu Y, Niu Y, Li J, Ye L, Kong J et al. (2016). Petrogenesis and tectonic significance of the late Triassic mafic dykes and felsic volcanic rocks in the East Kunlun Orogenic Belt, Northern Tibet Plateau. Lithos 245: 205-222.

Jenner G, Foley S, Jackson S, Green T, Fryer B, Longerich H (1993). Determination of partition coefficients for trace elements in high pressure-temperature experimental run products by laser ablation microprobe-inductively coupled plasma-mass spectrometry (LAM-ICP-MS). Geochimica et Cosmochimica Acta 57: 5099-5103.

Jiang C, An S (1984). On chemical characteristics of calcific amphiboles from igneous rocks and their petrogenesis significance. Journal of Mineralogy and Petrology 3: 1-9.

Johnson MC, Rutherford MJ (1989). Experimental calibration of the aluminum-in-hornblende geobarometer with application to Long Valley caldera (California) volcanic rocks. Geology 17: 837-841.

Kampunzu AB, Lubala RT (2012). Magmatism in extensional structural settings. the Phanerozoic African Plate, Springer-Verlag, 637 p.

Kay S.M, Mpodozis C, Tittler A, Cornejo P (1994). Tertiary magmatic evolution of the Maricunga mineral belt in Chile. International Geology Review 36: 1079-1112.

Kimura JI, Yoshida T (2006). Contributions of slab fluid, mantle wedge and crust to the origin of Quaternary lavas in the NE Japan arc. Journal of Petrology 47: 2185-2232.

Kornprobst J, Ohnenstetter D, Ohnenstetter M (1981). Na and Cr contents in clinopyroxenes from peridotites: a possible discriminant between "sub-continental" and "sub-oceanic" mantle. Earth and Planetary Science Letters 53: 241-254.

Kretz R (1983). Symbols for rock-forming minerals. American Mineralogist 68: 277-279.

Kretz R (1994). Metamorphic Crystallization. Wiley, 530p.

Le Bas MJ (1962). The role of aluminum in igneous clinopyroxenes with relation to their parentage. American Journal of Science 260: 267-288.

Le Maitre RWB, Dudek P, Keller A, Lameyre J, Le Bas J et al. (1989). A classification of igneous rocks and glossary of terms: Recommendations of the International Union of Geological Sciences, Subcommission on the Systematics of Igneous Rocks. International Union of Geological Sciences.

McDonough WF, Sun SS (1995). The composition of the Earth. Chemical Geology 120: 223-253.

Moghadam HS, Stern RJ, Chiaradia M, Rahgoshay M (2013). Geochemistry and tectonic evolution of the Late Cretaceous Gogher–Baft ophiolite, central Iran. Lithos 168: 33-47.

Mohr PA (1987). Crustal contamination in mafic sheets: a summary, Mafic Dyke Swarms. Geological Association of Canada Special Paper 34: 75-80.

Morimoto N (1988). Nomenclature of pyroxenes. Mineralogy and Petrology 39: 55-76.

Münker C (1998). Nb/Ta fractionation in a Cambrian arc/back arc system, New Zealand: source constraints and application of refined ICP-MS techniques. Chemical Geology 144: 23-45.

NBr ST, Son AM (1992). Sieve-textured plagioclase in volcanic rocks produced by rapid decompression. American Mineralogist 77: 1242-1249.

Nimis P (1999). Clinopyroxene geobarometry of magmatic rocks. Part 2. Structural geobarometers for basic to acid, tholeiitic and mildly alkaline magmatic systems. Contributions to Mineralogy and Petrology 135: 62-74.

Nimis P, Taylor WR (2000). Single clinopyroxene thermobarometry for garnet peridotites. Part I. Calibration and testing of a Cr-in-Cpx barometer and an enstatite-in-Cpx thermometer. Contributions to Mineralogy and Petrology 139: 541-554.

Nisbet EG, Pearce JA (1977). Clinopyroxene composition in mafic lavas from different tectonic settings. Contributions to Mineralogy and Petrology 63: 149-160.

Otten MT (1984). The origin of brown hornblende in the Artfjället gabbro and dolerites. Contributions to Mineralogy and Petrology 86: 189-199.

Pandey A, Rao NC, Chakrabarti R, Pandit D, Pankaj P et al. (2017). Petrogenesis of a Mesoproterozoic shoshonitic lamprophyre dyke from the Wajrakarur kimberlite field, eastern Dharwar craton, southern India: Geochemical and Sr-Nd isotopic evidence for a modified sub-continental lithospheric mantle source. Lithos 292: 218-233.

Pearce JA (1982). Trace element characteristics of lavas from destructive plate boundaries. In book: Andesites: Orogenic Andesites and Related Rocks, Edited by RS Thorpe, John Wiley and Sons, 528-548.

Pearce JA, Norry MJ (1979). Petrogenetic implications of Ti, Zr, Y, and Nb variations in volcanic rocks. Contributions to Mineralogy and Petrology 69: 33-47.

Plank T (2005). Constraints from thorium/lanthanum on sediment recycling at subduction zones and the evolution of the continents. Journal of Petrology 46: 921-944.

Putirka K (1996). Thermobarometry of mafic igneous rocks based on clinopyroxene-liquid equilibria, 0–30 kbar. Contributions to Mineralogy and Petrology 123: 92-108.

Putirka K (2008). Thermometers and barometers for volcanic systems. Reviews in mineralogy and geochemistry 69: 61-120.

Putirka K, Ryerson F, Mikaelian H (2003). New igneous thermobarometers for mafic and evolved lava compositions, based on clinopyroxene+ liquid equilibria. American Mineralogist 88: 1542-1554.

Rasouli J, Ghorbani M, Ahadnejad V (2014). Field observations, Petrography and microstructures study of Jebale Barez Plutonic complex (East-North East Jiroft). Journal of Tethys 2: 178-195.

Robinson PT, Malpas J, Dilek Y, Zhou M (2008). The significance of sheeted dyke complexes in ophiolites. GSA Today 18: 4-10.

Rudnick R, Gao S (2003). Composition of the continental crust. Treatise on Geochemistry 3: p 659.

Saccani E, Azimzadeh Z, Dilek Y, Jahangiri A (2013). Geochronology and petrology of the Early Carboniferous Misho Mafic Complex (NW Iran), and implications for the melt evolution of Paleo-Tethyan rifting in Western Cimmeria. Lithos 162: 264-278.

Sarjoughian F, Kananian A (2017). Zircon U-Pb geochronology and emplacement history of intrusive rocks in the Ardestan section, central Iran. Geologica Acta 15: 0025-0036.

Schmidt MW (1992) Amphibole composition in tonalite as a function of pressure: an experimental calibration of the Al-in-hornblende barometer. Contributions to Mineralogy and Petrology 110: 304-310.

Shafiei B, Haschke M, Shahabpour J (2009). Recycling of orogenic arc crust triggers porphyry Cu mineralization in Kerman Cenozoic arc rocks, southeastern Iran. Mineralium Deposita 44: 265-283.

Shahabpour J (2005). Tectonic evolution of the orogenic belt in the region located between Kerman and Neyriz. Journal of Asian Earth Sciences 24: 405-417.

Soesoo A (1997). A multivariate statistical analysis of clinopyroxene composition: Empirical coordinates for the crystallization PT-estimations. GFF 119: 55-60.

Sohrabi A, Beygi S, Nadimi A, Hajihashemi M (2015). The role of regional tectonics in structural caves, Simorgh Cave, Sofeh Mountain (Iran). Journal of Tethys 3: 114-122.

Stöcklin J (1974). Possible ancient continental margins in Iran, The geology of continental margins. Springer 873-887.

Stocklin J, Nabavi M (1973). Tectonic map of Iran. Geological Survey of Iran.

Sun SS, McDonough WS (1989). Chemical and isotopic systematics of oceanic basalts: implications for mantle composition and processes. Geological Society, London, Special Publications 42: 313-345.

Swinden HS, Jenner G, Kean B, Evans D (1989). Volcanic rock geochemistry as a guide for massive sulphide exploration in central Newfoundland. Current Research. Newfoundland Department of Mines 201-219.

Taylor B, Martinez F (2003). Back-arc basin basalt systematics. Earth and Planetary Science Letters 210: 481-497.

Torabi G (2010). Early Oligocene alkaline lamprophyric dykes from the Jandaq area (Isfahan Province, Central Iran): Evidence of Central–East Iranian microcontinent confining oceanic crust subduction. Island Arc 19: 277-291.

Torabi G (2011). Late Permian blueschist from Anarak ophiolite (Central Iran, Isfahan province), a mark of multi-suture closure of the Paleo-Tethys ocean. Revista Mexicana de Ciencias Geológicas 28: 544-554.

Vynhal C, McSween H, Speer J (1991). Hornblende chemistry in southern Appalachian granitoids: implications for aluminium hornblende thermobarometry and magmatic epidote stability. American Mineralogist 76: 176-188.

Wang C, Yang K, Xu Y, Cheng W (2009). Geochemistry and LA-ICP-MS Zircon U-Pb age of basic dyke swarms in north Daba Mountains and its tectonic significance. Geological Science and Technology Information 28: 19-26.

Weaver BL, Tarney J (1984). Empirical approach to estimating the composition of the continental crust. Nature 310: 575-577.

Wilson M (1989). Igneous Petrogenesis: A Global Tectonic Approach. Unwin Hyman, London 466 p.

Winchester J, Floyd P (1977). Geochemical discrimination of different magma series and their differentiation products using immobile elements. Chemical Geology 20: 325-343.

Wood DA (1980). The application of a Th-Hf-Ta diagram to problems of tectonomagmatic classification and to establishing the nature of crustal contamination of basaltic lavas of the British Tertiary Volcanic Province. Earth and Planetary Science Letters 50: 11-30.

Xu W, Li C, Wang M, Fan JJ, Wu H, Li X (2017). Subduction of a spreading ridge within the Bangong Co–Nujiang Tethys Ocean: Evidence from Early Cretaceous mafic dykes in the Duolong porphyry Cu–Au deposit, western Tibet. Gondwana Research 41: 128-141.

Xu Z, Han BF, Ren R, Zhou YZ, Zhang L et al. (2012). Ultramafic–mafic mélange, island arc and post-collisional intrusions in the Mayile Mountain, West Junggar, China: implications for Paleozoic intra-oceanic subduction–accretion process. Lithos 132: 141-161.

Yang JH, Sun JF, Chen F, Wilde SA, Wu FY (2007). Sources and petrogenesis of Late Triassic dolerite dykes in the Liaodong Peninsula: Implications for post-collisional lithosphere thinning of the eastern North China Craton. Journal of Petrology 48: 1973-1997.

Zhao Z, Mo X, Dilek Y, Niu Y, DePaolo DJ et al. (2009). Geochemical and Sr–Nd–Pb–O isotopic compositions of the post-collisional ultrapotassic magmatism in SW Tibet: petrogenesis and implications for India intra-continental subduction beneath southern Tibet. Lithos 113: 190-212.